Beamspace Modulated Circular Array

Chepala, A., Tataria, H., & Fusco, V. (2019). Beamspace Modulated Circular Array. *IEEE Transactions on Antennas and Propagation*. https://doi.org/10.1109/TAP.2019.2901092

Published in:
IEEE Transactions on Antennas and Propagation

Document Version:
Peer reviewed version

This article has been accepted for publication in a future issue of this journal, but has not been fully edited. Content may change prior to final publication. Citation information: DOI 10.1109/TAP.2019.2901092, IEEE Transactions on Antennas and Propagation

Beamspace Modulated Circular Array

Anil Chepala, Harsh Tataria, and Vincent Fusco, *Fellow, IEEE*

***Abstract*—In this paper, we show how each independent spatial mode of a circular array can be individually encoded and collimated to yield high ergodic spectral sum efficiency of an uplink mobile communication system. We show that every mode generated with the help of Rotman Lens is orthogonal to every other mode. This reduces the spatial cross-coupling and thereby enhances data throughput. We also show that unlike other phased arrays, the circular array has the ability to detect direction of arrival (DOA) from the backward half-space of the array to advantage. Furthermore, we show that because of its symmetry, the array can unlike linear arrays, create beam that can be scanned over 360° in azimuth scan plane. A proof of principle multi-mode circular array (MMCA) for the purpose defined above is designed, simulated and tested.**

***Index Terms*—Circular Array, Envelope Correlation Coefficient, Ergodic Sum Spectral Efficiency.**

I. Introduction

An advantage of circular arrays is their far-field radiation pattern symmetry, which can be exploited in order to electronically scan a beam 360° with minimal variations in the gain and pattern shape [1]–[5]. This far-field pattern can be expressed as summation of individual component patterns called *mode* patterns. A *mode* is a unique set of excitation surface current that radiates to generate corresponding unique *mode* pattern. A combination of these *mode* patterns represents the far-field radiation pattern of the circular array. The synthesis of these spatial *modes* using beamforming networks was presented by Sheleg [1]. These *modes* have the special property that they are spatially *orthogonal* to each other, which we exploit here in order to enhance the data throughput in the channel. Here we use a Rotman lens (RL) beamformer for exciting the *modes* and evaluate their *orthogonality* by computing the Envelope Correlation Coefficient (ECC) [6]. When each of these modes are encoded induvidually and transmitted, we show that the ergodic sum spectral efficiency (ESSE) of an uplink mobile communication system can be improved.

The aim of this paper is to demonstrate how each mode of a circular array (CA) can be separately encoded and collimated to increase cellular system spectral efficiency, as well as spatial coverage. The theoretical aspects of single and multiple beam operation of a CA are discussed in Section II. Section III describes the novel contribution of this paper, wherein, each individual mode of the CA when independently excited can be used to provide N (the number of radiating elements in the CA) orthogonal modes, each of which is capable of carrying its own data stream. This is illustrated by showing that even when a physical Rotman lens (RL) is used for beamforming the resulting radiation patterns have low envelope correlation coefficients (ECC). Consequently, this opens the way for enhancing cellular system spectral efficiency. Section IV describes the available spectral efficiency estimates for a multiple user multiple-input-multiple-output (MU-MIMO) situation. Finally, Section V concludes the paper.

This work was supported by Queens University Belfast Scholarship and EPSRC under the grants EP/P000673/1, EP/N020391/1.

A. Chepala and V. Fusco are with the Institute of Electronics, Communications, and Information Technology(ECIT),Queen's University Belfast, BT3 9DT, UK (e-mail: achepala01@qub.ac.uk and v.fusco@ecit.qub.ac.uk).

H. Tataria was with the Institute of Electronics, Communications, and Information Technology(ECIT),Queen's University Belfast, BT3 9DT, UK. He is now with the Department of Electrical and Information Technology, Lund University, SE22100, Lund, Sweden (e-mail: harsh.tataria@eit.lth.se)

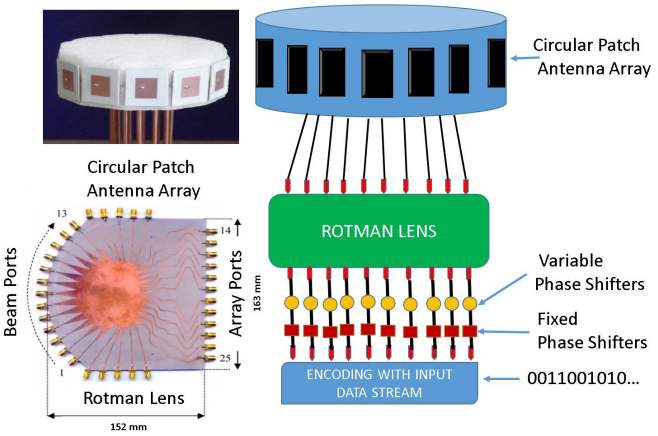

Fig. 1. Multimode circular array architecture.

II. Circular Array Operation and Multiple Beam Forming

The classical architecture of a CA (see Fig.1)in transmit mode is described in [1], [4], [5], as well as references therein. The mode basis for operation of a CA can be understood by considering a continuous current distribution, [1]. The horizontal far-field pattern $F(\phi)$ of a continuous circular aperture is a periodic function repeating on 2π. Mathematically it can therefore be expressed as a complex Fourier series that is a function of both amplitude and phase.

$$F(\phi) = \sum_{-M}^{M} C_m \; e^{jm\phi}, for - M \leq m \leq -M, \qquad (1)$$

This represents the transmit operation of the CA. where m mode number is an integer and M is the highest mode index. In case of receive operation the mode excitations can be computed by

$$C_m = \int_0^{2\pi} F(\phi) \; e^{-jm\phi} \qquad (2)$$

ϕ = azimuth angle and m = mode number

If $B_K \; e^{j\beta_k}$ is the current applied to the $K-$th input port of a beamforming network, the outputs of which are connected to

This article has been accepted for publication in a future issue of this journal, but has not been fully edited. Content may change prior to final publication. Citation information: DOI 10.1109/TAP.2019.2901092, IEEE Transactions on Antennas and Propagation

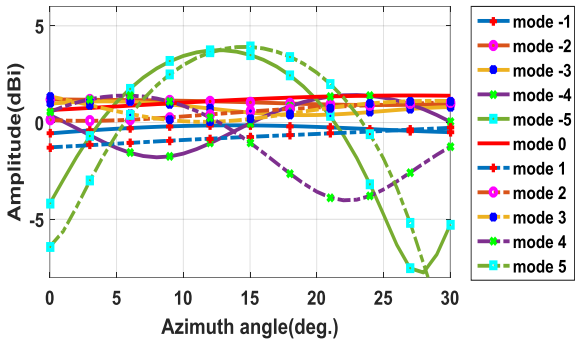

(a)

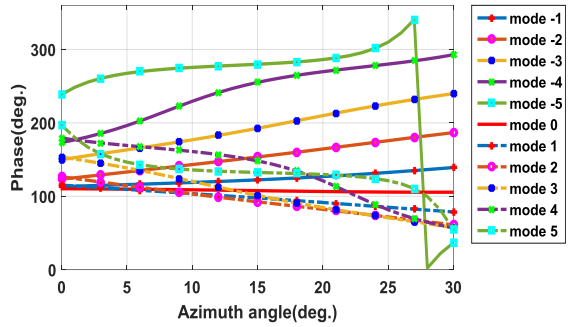

(b)

Fig. 2. Simulated CA mode response when excited with phase ramp. (a) Amplitudes and (b) Phases of modes for the structure.

the CA elements, the resultant $A_J\ e^{j\beta_J}$ on the $J-$th radiating element is given by

$$A_J\ e^{j\beta_J} = \frac{1}{\sqrt{N}} B_K\ e^{j\beta_k}\ e^{jKJ(2\pi/N)} \tag{3}$$

Fig. 2 shows the simulated modes for a 9.3 GHz 12-element CA prototype consisting of coaxially fed microstrip patch elements chosen for physical compactness and ease of manufacturing, each with better than 10 dB return loss. These are arranged around a 60 mm diameter circle as shown in Fig. 1. Each of the modes in Eq. (3) can be excited independently by applying a suitable $m \times 360/N$ phase ramp to the radiating elements where m is the mode number and N is the total number of elements in the CA. This is readily acheived by feeding the beamports of a RL [7], due to its simple 2D realization in microstrip technology.

A. Combined modes using Rotman Lens

The modes on a circular array are excited by using a RL. Each RL beam port excitation generates an individual mode on the array. The modes exhibit linear phase response up to mode 4 with the higher order modes having greater amplitude ripple and less linear phase responses. *Hence, only modes up to ±4 are used for encoding when beamforming.*

The modes once phase aligned [5] can be combined to beam form by simultaneously exciting multiple beam port pairs on the RL. This combination and the sequential addition of the mode pairs results in increased collimation of the beam formed.

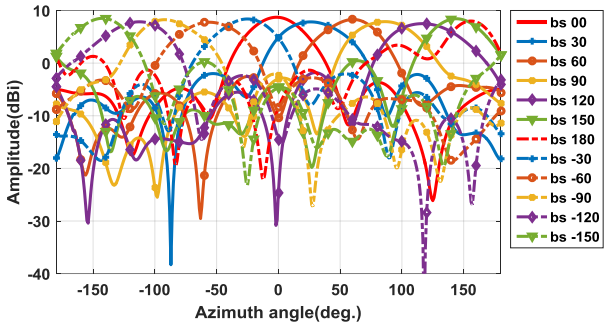

Fig. 3. Beamsteering using phase ramp on CA-12 with RL.

B. Beamsteering Using Rotman Phase Ramp

The formed beam can be steered in azimuth by providing a phase ramp at the input of the RL [7]. This phase ramp when applied at the inputs of the RL, using variable phase shifters, will produce corresponding rotation in the far-field as shown in Fig. 3. The CA with RL is a linear system and it is therefore possible to form multiple orthogonal beams simultaneously in desired directions through superposition of steering vectors.

III. Mode Orthogonality of the Circular Array using a Rotman Lens Beamformer

Next, we check the *orthogonality* between the measured far-field patterns associated with each circular array mode, which is a necessary requirement for minimizing spatial cross coupling between imprinted data streams as a means for enhancing data throughput. This is done by calculating the ECC [6], of each of the CA modes. $\bar{F}_1$ and $\bar{F}_2$ are the far-field radiation patterns whose orthogonality is evaluated by computing ECC as given in equation below

$$\rho_e = \frac{|\int\int_{4\pi} \left[\bar{F}_1(\theta,\phi) \cdot \bar{F}_2^{\star}(\theta,\phi)\ d\Omega\right]|^2}{\int\int_{4\pi} |\bar{F}_1(\theta,\phi)|^2 d\Omega \cdot \int\int_{4\pi} |\bar{F}_2(\theta,\phi)|^2 d\Omega}. \tag{4}$$

The 3D far-field patterns for each of the modes from the simulation are recorded at 9.3 GHz and ρ_e is computed. In Table-I, the peak along the diagonal represents the auto correlation and the other positions represent the cross-correlation between the mode patterns. The ECC when computed at frequencies around the design centre frequency suggest that 22% correlation bandwidth should be achievable for $\rho_e \leq 0.02$.

IV. Ergodic Sum Spectral Efficiency Evaluations

The global symmetry in the far–field radiation pattern of CAs can be exploited to direct/receive electromagnetic energy into/from a particular cluster of scatterers in the far–field. Due to this reason, circular arrays naturally complement cellular communication applications, where we have a fixed centralized array at the base station (BS) providing simultaneous service to a multiplicity of non–cooperative randomly positioned mobile terminals in the same time, over the same frequency.Next we consider the uplink of a multiuser multiple–input multiple–output system operating in an urban macrocellular environment. Specifically, we consider the case where the BS

This article has been accepted for publication in a future issue of this journal, but has not been fully edited. Content may change prior to final publication. Citation information: DOI 10.1109/TAP.2019.2901092, IEEE Transactions on Antennas and Propagation

TABLE I
MEASURED ECC OF MODE PATTERNS IN CA

ECC @ 9.3 GHz (*each value is 100 × ECC)													
	bp-1	bp-2	bp-3	bp-4	bp-5	bp-6	bp-7	bp-8	bp-9	bp-10	bp-11	bp-12	bp-13
bp-1	100	48.06	0.05	4.13	0.56	2.08	0.10	0.01	0.12	0.30	1.36	1.19	0.03
bp-2	48.06	100	31.89	0.67	1.86	1.91	0.27	0.13	1.53	0.82	1.46	1.37	1.62
bp-3	0.05	31.89	100	23.84	2.47	1.08	4.01	1.07	0.18	12.02	0.98	1.39	1.01
bp-4	4.13	0.67	23.84	100	27.52	2.19	0.24	2.07	0.46	0.58	0.64	0.56	0.59
bp-5	0.56	1.86	2.47	27.52	100	24.8	0.9	0.96	0.50	0.49	0.24	2.10	0.33
bp-6	2.08	1.91	1.08	2.19	24.87	100	13.12	0.79	0.38	2.24	0.96	0.03	0.02
bp-7	0.10	0.27	4.01	0.24	0.95	13.12	100	12.86	0.93	0.45	2.60	0.35	0.14
bp-8	0.01	0.13	1.07	2.07	0.96	0.79	12.86	100	26.31	1.96	1.07	1.54	2.04
bp-9	0.12	1.53	0.18	0.46	0.50	0.38	0.93	26.31	100	27.45	1.82	2.66	0.60
bp-10	0.30	0.82	12.02	0.58	0.49	2.24	0.45	1.96	27.45	100	24.53	0.60	4.63
bp-11	1.36	1.46	0.98	0.64	0.24	0.96	2.6	1.07	1.82	24.53	100	32.45	0.15
bp-12	1.19	1.37	1.39	0.56	2.10	0.03	0.35	1.54	2.66	0.60	32.45	100	46.21
bp-13	0.03	1.62	1.01	0.59	0.33	0.02	0.14	2.04	0.60	4.63	0.15	46.21	100

is equipped with a circular array of N antenna elements, receiving independent data streams from L single–antenna terminals ($L \ll N$). The terminals are uniformly distributed in a coverage area of the BS with a radius $\mathbf{R_c}$, where the BS is located at the origin of this circle. The transceiver unit at the BS is implemented in this case via a RL, while for simplicity, the baseband combiner is implemented via a maximum–ratio combining. Since each terminal has a single receive antenna, one RF chain is assumed at each terminal, in contrast to the L RF chains assumed at the BS to demultiplex L data streams at a given time instance.

Keeping the above in mind, we model the $N \times 1$ uplink propagation channel between terminal $k \in 1, 2, \ldots, L$ and the BS via the classical double–directional channel description given by [8]

$$\mathbf{h}_k = \frac{1}{\sqrt{CL_p}} \sum_{c=1}^{C} \sum_{\ell=1}^{L_p} \alpha_{c,\ell}^{(k)} \, \mathbf{a}_{\text{BS}}^{(k)} (\phi_{c,\ell}) \,, \tag{5}$$

where C denotes the total number of scattering clusters and L_p denotes the number of contributing multipath components (MPCs) within each cluster. Note that both C and L_p are frequency sensitive constants, and are primarily a random functions of the surrounding radio environment. Furthermore, $\alpha_{c,\ell}^{(k)}$ denotes the complex gain of the l–th MPC belonging to the c–th scattering cluster from terminal k, which is scaled by the large–scale propagation effects of geometric attenuation and shadow fading at the link distance r_k. More precisely, we model $\alpha_{c,\ell}^{(k)} \sim \mathcal{CN}(0, \beta_k)$, where $\beta_k = r_k^{-\gamma} \xi_k$. Note that γ is the attenuation exponent and ξ_k follows a lognormal random distribution such that $10 \log_{10}(\xi_k) \sim \mathcal{N}\left(0, \sigma_{\text{s}}^2\right)$.[1] Further to this, $\mathbf{a}_{\text{BS}}^{(k)}$ denotes the $N \times 1$ far–field array steering response vector of the CA at the instantaneous azimuth direction–of–arrival (DOA), $\phi_{c,\ell}$. Note that the precise structure of $\mathbf{a}_{\text{BS}}^{(k)}$ was obtained from full–wave electromagnetic evaluations for $N = 12$ element 9.3 GHz CA discussed in the earlier sections of the manuscript. We also consider the case of a linear array interfaced with the same signal processing unit. We choose that the aperture of both circular and linear arrays are equivalent. For the case of a linear array, $\mathbf{a}_{\text{BS}}^{(k)}$ is well known to follow

$$\mathbf{a}_{\text{BS}}^{(k)} (\phi_{c,\ell}) = \frac{1}{\sqrt{N}} \left[1, e^{j \frac{2\pi}{\lambda} \Delta \kappa_{\phi_{c,\ell}}}, \ldots, e^{j \frac{2\pi}{\lambda} \Delta (N-1) \kappa_{\phi_{c,\ell}}}\right]^T \tag{6}$$

where $\kappa_{\phi_{c,\ell}} = \sin(\phi_{c,\ell}) \; \Delta$ denotes the electrical inter–element spacing between two elements and λ is the operational wavelength.[2]. Since N fixed analog beams can be formed at the BS via the use of a RL, we denote the spatial azimuth beamsteering angles as $\varphi_1, \varphi_2, \ldots, \varphi_N$. Since $L \ll N$, the L user terminals are "selected" via a bank of RF switches, occupying L distinct subports of the Rotman beamport contour, due to L random DOAs. The dimension–reduced signal after beam selection is downconverted via L RF transceivers and digitized before baseband combining with maximum–ratio processing. The resulting $L \times 1$ composite received signal after beam selection is given by

$$\mathbf{y} = \rho^{\frac{1}{2}} \mathbf{S}_{\text{RF}} \mathbf{F}_{\text{RF}} \mathbf{H} \mathbf{x} + \mathbf{n} = \rho^{\frac{1}{2}} \mathbf{G} \mathbf{x} + \mathbf{n}, \tag{7}$$

where $\mathbf{G} = [\mathbf{g}_1 \, \mathbf{g}_2, \ldots, \mathbf{g}_L]$ is an $L \times L$ matrix such that the $L \times 1$ vector $\mathbf{g}_k = \mathbf{S}_{\text{RF}} \mathbf{F}_{\text{RF}} \mathbf{h}_k$, $\forall k = 1, 2, \ldots, L$. Now, $\rho^{\frac{1}{2}} \mathbf{x}$ is the $L \times 1$ vector of uplink payload data, where the average transmit power of each terminal is ρ, with $\mathbb{E}[|x_k|^2] = 1, \forall k = 1, 2, \ldots, L$.[3] The net functionality of the Rotman lens can be described by the $N \times N$ matrix, $\mathbf{F}_{\text{RF}}$, such that $\mathbf{F}_{\text{RF}} = \left[\mathbf{a}_{\text{BS}}^H(\varphi_1) \;\; \mathbf{a}_{\text{BS}}^H(\varphi_2), \ldots, \mathbf{a}_{\text{BS}}^H(\varphi_N)\right]^T$, where the precise form of each vector is obtained from full–wave electromagnetic analysis. The directions $\varphi_1, \varphi_2, \ldots, \varphi_L$ (corresponding to L terminals), are then selected via an $L \times N$ RF switching network, $\mathbf{S}_{\text{RF}}$. With an ideally operating RF switch, $\mathbf{S}_{\text{RF}}$ is a binary matrix, where each row of the matrix contains only one non–zero entry corresponding to the selected beam index at a given subport. The $L \times 1$ vector of additive Gaussian noise is denoted by $\mathbf{n}$, where each entry of $\mathbf{n} \sim \mathcal{CN}(0, 1)$. From the composite received signal in (7), the signal–to–interference–plus–noise–ratio (SINR) of terminal k with maximum–ratio baseband processing is given by

$$\text{SINR}_k = \frac{\rho \left|\mathbf{g}_k^H \mathbf{g}_k\right|^2}{\sigma^2 \mathbf{g}_k^H \mathbf{g}_k + \rho \sum_{\substack{i=1 \\ i \neq k}}^{L} \left|\mathbf{g}_k^H \mathbf{g}_i\right|^2}. \tag{8}$$

[1]The mathematical notation $x \sim \mathcal{CN}\left(0, \sigma^2\right)$ reads as x follows a Gaussian random variable with zero–mean and variance σ^2.

[2]The mathematical notation $(\cdot)^T$ is a vector transpose operation.

[3]Here, $\mathbb{E}[\cdot]$ denotes the statistical expectation.

This article has been accepted for publication in a future issue of this journal, but has not been fully edited. Content may change prior to final publication. Citation information: DOI 10.1109/TAP.2019.2901092, IEEE Transactions on Antennas and Propagation

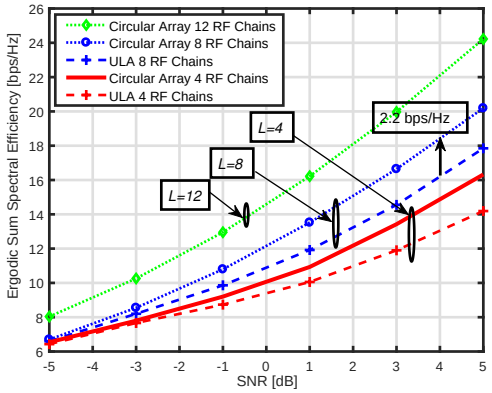

Fig. 4. Ergodic sum spectral efficiency of beamspace modulated circular arrays and ULAs with hybrid signal processing. Analog processing is carried out via a RL, while baseband processing is carried out via maximum–ratio combining. Note that the number of RF chains are 4 or 8 to compare the relative performance benefits of the circular array.

For a given instance of $\mathbf{g}_k$ and $\mathbf{g}_i$, SINR_k can be translated into an instantaneous spectral efficiency (in bit/sec/Hz) for terminal k via the classical Shannon formulation of $\text{R}_k = \log_2(1+\text{SINR}_k)$. This can be used to compute the ergodic sum spectral efficiency across all L terminals over the small–scale fading in the individual MPCs as $\text{R}_{\text{sum}} = \mathbb{E}[\sum_{k=1}^{L} \text{R}_k]$. For further discussion on any of the above modelling methods, see [9]. The numerical parameters for our subsequent evaluations are chosen from the standardized propagation channel model released by the Third Generation Partnership Project (3GPP) at microwave frequencies in [10]. Consistent with [10], we set $C = L_p = 20$. Our evaluations assume a coverage radius $R_{\text{c}} = 500$ m with a geometric attenuation exponent $\gamma = 3.67$ and shadow fading standard deviation $\sigma_{\text{s}} = 6$ dB. Each terminal is assumed to operate with the same uplink transmit power, while the noise power at the BS array is $\sigma^2 = 1$. This implies that ρ is the average operating signal–to–noise–ratio (SNR). For the beam selection at the RL, $\varphi_k = (k-1)\,2\pi/N$, $\forall k = 1, 2, \ldots, N$. The far–field steering response of a uniform linear array (ULA) is utilized with a uniform beam scanning range within the forward half–space of the array. Each of the following results are generated with 10^5 Monte–Carlo simulation realizations of the multiuser system. Fig. 4 depicts the ergodic sum spectral efficiency as a function of the uplink operating SNR. Three trends can be noted: First is the fact that increasing the number of RF chains from 4 to 8 yields an increase in the ergodic sum spectral efficiency, since we can demultiplex twice the number of data streams and in turn support twice the number of mobile terminals. This applies equally to both circular and linear arrays, respectively. Secondly, when the number of RF chains are 4 and 8, the CA offers greater ergodic sum spectral efficiency relative to the linear array, due to its ability to detect uplink DOAs from the backward halfspace of the array. In addition, with the RL as the beamforming network, the CA has the additional benefit of focusing the received gain "equally" in all directions around the 360° azimuth scan plane. On average, at a moderately high SNR of 4 dB, one can note a 2.2 bps/Hz difference in the spectral efficiency.Thirdly, for both 4 and 8 RF chains, the differences in the predicted spectral efficiency from circular and linear arrays are seen to grow with SNR, since the spatial multiplexing gain of the system is dominated by the high SNR regime, where the levels of interference also start to increase. It is noteworthy that the case of 12 RF chains serves as a useful upper bound on the predicted performance,for the example system, here naturally much higher ergodic spectral efficiencies are observed. In contrast to the results in Fig. 4, the spectral efficiency obtained using an ideal modal beamformer yields 2.2 bps/Hz higher capacity than afforded by the RL.

V. Conclusions

We have shown that it is possible to exploit the individual modes of a CA in order to enhance the capacity of a wireless system over that which can be achieved by using a ULA both in terms of capacity and field of view. This is achieved through mode spatially diversity. The use of a RL to provide the mode excitation requirement has been shown to be effective and provides a simple means for physical implementation. The approach suggested offers the possibility for improved wireless transmission systems with 360° of look angle.

Acknowledgments

The authors would like to acknowledge the support given by Queens University Belfast Scholarship and to the EPSRC under the grants EP/P000673/1, EP/N020391/1. The authors would also like to thank Mr. Kieran Rainey for fabrication and testing of the CA.

References

[1] B. Sheleg, "A matrix-fed circular array for continuous scanning," *Proceedings of the IEEE*, vol. 56, no. 11, pp. 2016–2027, Nov. 1968.

[2] I. D. Longstaff, P. E. K. Chow, and D. E. N. Davies, "Directional properties of circular arrays," *Electrical Engineers, Proceedings of the Institution of*, vol. 114, no. 6, pp. 713–718, Jun 1967.

[3] W. R. Lepage, C. S. Roys, and S. Seely, "Radiation from circular current sheets," *Proceedings of the IRE*, vol. 38, no. 9, pp. 1069–1072, Sept. 1950.

[4] D. E. N. Davies and B. S. McCartney, "Cylindrical arrays with electronic beam scanning," *Electrical Engineers, Proceedings of the Institution of*, vol. 112, no. 3, pp. 497–505, Mar. 1965.

[5] T. Rahim, *Directional pattern synthesis in circular arrays of directional antennas*. PhD Dissertation, University College London, Aug. 1980.

[6] A. Ourir, K. Rachedi, D. T. Phan-Huy, C. Leray, and J. de Rosny, "Compact reconfigurable antenna with radiation pattern diversity for spatial modulation," in *2017 11th European Conference on Antennas and Propagation (EUCAP)*, Mar. 2017, pp. 3038–3043.

[7] Y. Zhang, S. Christie, V. Fusco, R. Cahill, G. Goussetis, and D. Linton, "Reconfigurable beam forming using phase-aligned rotman lens," *IET Microwaves, Antennas Propagation*, vol. 6, no. 3, pp. 326–330, Feb. 2012.

[8] M. Steinbauer, A. F. Molisch, and E. Bonek, "The double-directional radio channel," *IEEE Antennas and Propagation Magazine*, vol. 43, no. 4, pp. 51–63, Aug. 2001.

[9] H. Tataria, M. Matthaiou, P. J. Smith, G. C. Alexandropoulos, and V. F. Fusco, "Impact of rf processing and switching errors in lens-based massive mimo systems," in *2018 IEEE 19th International Workshop on Signal Processing Advances in Wireless Communications (SPAWC)*, Jun. 2018, pp. 1–5.

[10] 3GPP TR 36.873 v.12.2.0, *Study on 3D channel models for LTE*. 3GPP, Jun. 2015.